One-shot Hyperspectral Imaging using Faced Reflectors

Tsuyoshi Takatani† Takahito Aoto‡ Yasuhiro Mukaigawa†
†Nara Institute of Science and Technology ‡National Institute of Informatics
{takatani.tsuyoshi.to2, mukaigawa}@is.naist.jp aoto@nii.ac.jp

Abstract

Hyperspectral imaging is a useful technique for various computer vision tasks such as material recognition. However, such technique usually requires an expensive and professional setup and is time-consuming because a conventional hyperspectral image consists of a large number of observations. In this paper, we propose a novel technique of one-shot hyperspectral imaging using faced reflectors on which color filters are attached. The key idea is based on the principle that each of multiple reflections on the filters has a different spectrum, which allows us to observe multiple intensities through different spectra. Our technique can be implemented either by a coupled mirror or a kaleidoscope geometry. Experimental results show that our technique is capable of accurately capturing a hyperspectral image by using a coupled mirror setup which is readily available.

1. Introduction

A hyperspectral image includes valuable information which is useful for various computer vision tasks such as material recognition [29], color consistency [3], and anomaly detection [27]. However, conventional hyperspectral imaging requires an expensive and professional system that is not easily available. Most commercial hyperspectral cameras capture a scene multiple times with a large number of narrow band filters or a tunable narrow band filter. Since a narrow band filter allows the spectral light at a certain wavelength to pass through, it is possible to capture an image at the wavelength by attaching the filter in front of the camera. Multiple capturing with different narrow band filters enables us to obtain a hyperspectral image. Another commercial system employs dispersing the light into individual wavelengths by using a prism or a diffraction grating. Since the camera captures only the dispersed light on a 2D slice in the scene at a time, sweeping in the whole scene is necessary to obtain a hyperspectral image.

In this paper, we propose a novel technique of one-shot hyperspectral imaging using faced reflectors on which color filters are attached, as shown in Fig. 1. The light emitted from the light source is diffusely reflected on the target scene and then observed by the camera as an image. Moreover, the light after being reflected on the scene is also reflected on the reflectors before being observed by the camera. Thus, the spectrum of that observation is different from that without reflecting on the reflectors. That is, we can observe another image filtered by a different spectrum. On the faced reflectors, where the light is reflected multiple times, the light at each reflection is regarded as filtered by a different spectrum. Therefore, we can obtain multiple observations filtered by different spectra at once.

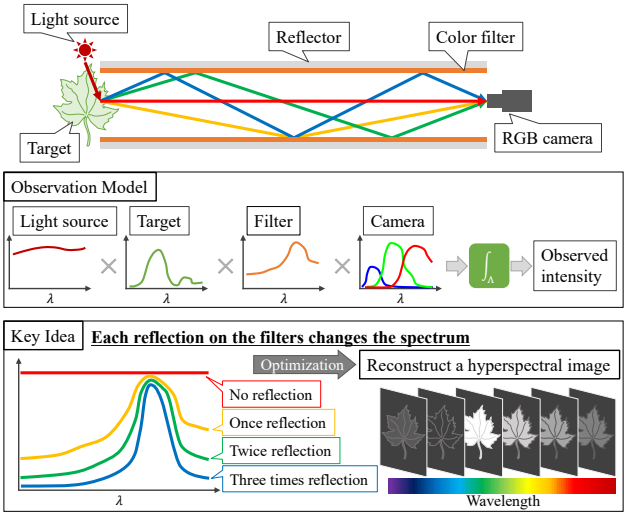

Figure 1: Overview of the proposed technique of one-shot hyperspectral imaging using faced reflectors. This simple setup employs a coupled mirror on which color filters are attached. Since the spectrum of the light varies at each reflection, we can obtain multiple observations from a single image. The observations allow us to reconstruct a hyperspectral image.

The technique can be implemented by various faced reflectors setup, such as a coupled mirror and a kaleidoscope geometry, as will be explained in Section 4. Our experimental results show that even a coupled mirror setup with only one kind of a color filter is capable of capturing a hyperspectral image whose reconstruction error is on average 14% on real data, as shown in Section 5.

1.1. Contributions

Our contributions are summarized as:

- *One-shot hyperspectral imaging:* Our technique is capable of capturing a hyperspectral image with one-shot by using a coupled mirror with only one kind of color filter, and its quantitative error is on average 14%.

- *Extremely low cost measurement system:* Implementing our technique only requires a pair of planar mirrors and a color filter, which are readily available for most users, and all of them totally cost less than $100.

2. Related work

We start by briefly reviewing the existing work for hyperspectral imaging. Traditional hyperspectral imaging employs a number of narrow band filters [28], a tunable narrow band filter [11, 21], and diffractive media [15, 8]. In general, methods based on a narrow band filter are time-consuming because it is necessary to capture a scene multiple times with a number of different filters. Methods based on diffractive media such as a grating and a prism also requires long time to capture a scene because its hyperspectral image consists of multiple columns obtained by push-broom imaging. Most commercial hyperspectral cameras are based on those traditional approaches that are time-consuming and costly. To deal with those problems, there are many alternative approaches.

Computational photography There have been a number of methods for multispectral/hyperspectral imaging in computational photography. Most of the methods rely on active illumination. D'Zmura [9] recovered spectral reflectance through estimating coefficients in a linear model using a set of illumination patterns whose spectra are independent from each other. Park *et al*. [25] reconstructed a multispectral video by capturing a scene under multiplexed illumination which is combinations of different LEDs. Chi *et al*. [7] selected an optimized set of wide band filters to estimate spectral reflectance. They put the set of filters in front of a light source instead of a camera. Han *et al*. [14] proposed a method to fast recover the spectral reflectance by using a DLP projector and a high-speed camera. Instead of active illumination, Oh *et al*. [24] proposed a framework for reconstructing hyperspectral images by using multiple consumer-level digital cameras. They employed small differences of spectral sensitivities along multiple cameras for reconstructing a hyperspectral image. However multiple cameras are necessary to implement this method. Although those methods are very effective to make hyperspectral imaging more accurate and easier to be used, they still require expensive and specialized equipments.

One-shot hyperspectral imaging Several methods for one-shot hyperspectral imaging have been proposed. Morovic and Finlayson [22] proposed a method to estimate spectral reflectance from a single RGB image. It is impossible to establish a unique correspondence between an RGB vector and spectral reflectance because the dimension of reflectance is higher than that of an RGB vector. Therefore, they made strong assumptions that reflectance follows a normal probability distribution and is smooth, and then trained a model under some conditions to which reflectance must adhere. Abed *et al*. [2] proposed a linear interpolation method using lookup tables. In a case of a scene under the same illumination, the reflectance of a polytope that encloses an RGB point in the scene is used for interpolation. And Nguyen *et al*. [23] introduced a non-linear mapping strategy for modeling the mapping between an RGB value and a spectra. Those one-shot hyperspectral imaging techniques are effective to some extent but their accuracy highly rely on the dataset for training. Others for one-shot hyperspectral imaging are computed tomography image spectrometers [12], which obtains diffracted signals by slicing a hyperspectral image as a 3D data through a diffraction grating, and coded aperture snapshot spectral imagers [4], which employs compressive sensing by dispersive elements and a coded aperture. Both of the methods can estimate the 3D data from the diffracted signals but still require expensive and specialized equipments.

Kaleidoscope geometry Kaleidoscope geometry has often been used in computational photography. Han and Perlin [13] measured the bi-directional texture reflectance in a scene by using a kaleidoscope. Reshetouski *et al*. [26] introduced a framework for three-dimensional imaging using a kaleidoscope, and then implemented to obtain dense hemispherical multi-view data. Forbes *et al*. [10] reconstructed the shape of an object from silhouette by using a coupled mirror with an uncalibrated camera. Manakov *et al*. [20] proposed a camera add-on using a kaleidoscope for high dynamic range, multispectral, polarization, and light-field imaging. Their work looks similar to our idea but they copied the input image onto 3×3 images, and then used 9 selected color filters. On the other hand, our basic idea is to use only a color filter and put the filter on the reflectors, that is totally different from the work by Manakov *et al*.

3. One-shot hyperspectral imaging technique

3.1. Appearance model of faced reflectors

We first introduce the model to take an image by an RGB camera. We assume that isotropic spectral reflectance on the surface under a uniform illumination for a whole scene. An observed intensity y_k in the k-th channel of an image can

be expressed as

$$y_k = \int_\Lambda l(\lambda)s(\lambda)c_k(\lambda)d\lambda, \tag{1}$$

where λ is the wavelength, $l(\lambda)$ is the spectrum of the illumination, $s(\lambda)$ is the spectral reflectance, $c_k(\lambda)$ is the spectral sensitivity of the k-th channel on the camera, and Λ is the range of wavelength, for example, from 400 to 700nm if the visible light is assumed. When a pair of reflectors is placed between the scene and the camera as shown in Fig. 1, the light reflected in the scene is specularly reflected on the reflectors before being observed by the camera. Suppose that a color filter whose spectrum is $f(\lambda)$ is attached on both reflectors and the spectral reflectance of the reflector is flat, the observed intensity of the light once reflected on the reflector, see the yellow line in Fig. 1, can be expressed as

$$y_{k,1} = \int_\Lambda l(\lambda)s(\lambda)f(\lambda)c_k(\lambda)d\lambda. \tag{2}$$

When the light is twice reflected, shown as the green line in Fig. 1, it is multiplied by one more $f(\lambda)$. Regarding the light without reflection on the reflector, the red line in Fig. 1, as the case of $f^0(\lambda)$, the observed intensity $y_{k,i}$ to the i-bounce light reflected on the reflectors can be formulated as

$$y_{k,i} = \int_\Lambda l(\lambda)s(\lambda)f^i(\lambda)c_k(\lambda)d\lambda, \tag{3}$$

where $0 \leq i \leq N$ and N is the maximum number of bounces. N is an important factor to stably reconstruct the spectral reflectance and so we will discuss it in Section 3.3.

3.2. Problem formulation

The problem is here to estimate the spectral reflectance $s(\lambda)$ when all of the spectra of the light source $l(\lambda)$ and the color filter $f(\lambda)$ and the spectral sensitivities of the camera $c_k(\lambda)$ are known. To solve that, we transform Eq. 3 into a discrete formulation. The discrete formulation to Eq. 3 is

$$\begin{aligned} y_{k,i} &= \sum_{\lambda_b \leq \lambda \leq \lambda_e} l_\lambda s_\lambda f_\lambda^i c_{k,\lambda} \\ &= \sum_{\lambda_b \leq \lambda \leq \lambda_e} a_{k,i,\lambda} s_\lambda, \end{aligned} \tag{4}$$

where $a_{k,i,\lambda} \triangleq l_\lambda f_\lambda^i c_{k,\lambda}$, λ_b and λ_e are the minimum and maximum wavelengths in the range, respectively. Eq. 4 can be written in a matrix format as follows:

$$y_{k,i} = \boldsymbol{a}_{k,i}^{\mathrm{T}} \boldsymbol{s}, \tag{5}$$

where $\boldsymbol{a}_{k,i} = (a_{k,i,\lambda_b}, a_{k,i,\lambda_b+d\lambda}, \cdots, a_{k,i,\lambda_e})^{\mathrm{T}}$, $\boldsymbol{s} = (s_{\lambda_b}, s_{\lambda_b+d\lambda}, \cdots, s_{\lambda_e})^{\mathrm{T}}$, and $d\lambda$ is the granularity of wavelength in the discrete formulation. The resolution of wavelength is defined as $N_\lambda = \frac{\lambda_e - \lambda_b}{d\lambda}$. When all intensities of 3 channels and N bounces are measured, a simultaneous equation can be composed as

$$\boldsymbol{y} = \mathbf{A}\boldsymbol{s}, \tag{6}$$

where $\boldsymbol{y} = (y_{\mathrm{r},0}, y_{\mathrm{g},0}, y_{\mathrm{b},0}, y_{\mathrm{r},1}, \cdots, y_{\mathrm{b},N})^{\mathrm{T}} \in \mathbb{R}^{3N}$ and $\mathbf{A} = [\boldsymbol{a}_{\mathrm{r},0}, \boldsymbol{a}_{\mathrm{g},0}, \boldsymbol{a}_{\mathrm{b},0}, \boldsymbol{a}_{\mathrm{r},1}, \cdots, \boldsymbol{a}_{\mathrm{b},N}]^{\mathrm{T}} \in \mathbb{R}^{3N \times N_\lambda}$. Here, when the intensity vector $\boldsymbol{y}$ is observable and the coefficient matrix $\mathbf{A}$ is known, then the spectral reflectance $\boldsymbol{s}$ can be reconstructed as follows:

$$\hat{\boldsymbol{s}} = \arg\min_{\boldsymbol{s}} \|\mathbf{A}\boldsymbol{s} - \boldsymbol{y}\|^2. \tag{7}$$

When the rank of the coefficient matrix is sufficient, Eq. 7 can easily be solved by a conventional least squares technique.

3.3. The nature of the coefficient matrix A

The reconstruction of the spectral reflectance can be solved by a conventional least squares technique as mentioned in Section 3.2. However, the stability of its computation depends on the coefficient matrix $\mathbf{A}$. To obtain a stable solution, the rank of the coefficient matrix $\mathbf{A}$ has to be sufficient.

Furthermore, it is well known that the condition number of a problem is an important factor to stably solve the problem in the field of numerical analysis. A problem with a low condition number can stably be solved. In our formulation, the condition number of the problem is decided by the coefficient matrix as follows:

$$\kappa(\mathbf{A}) = \frac{\sigma_{\max}}{\sigma_{\min}}, \tag{8}$$

where $\sigma_{\max}, \sigma_{\min}$ are the maximum and minimum of singular values of $\mathbf{A}$, respectively. We define $\sigma_{\max} \triangleq \sigma_1$ and $\sigma_{\min} \triangleq \sigma_{\mathrm{rank}(\mathbf{A})}$.

Because we have assumed that the spectrum of the illumination l_λ, the spectral sensitivities of the camera $c_{k,\lambda}$, and the spectrum f_λ are all known, then the coefficient matrix $\mathbf{A}$ can be evaluated in advance. Therefore, when we have multiple color filters, it is possible to select the optimal color filter which make the rank sufficient and the condition number the lowest. We verify this nature in Section 5.2 by an experiment on synthetic data.

3.4. Constrained optimization

Although, as mentioned in Section 3.2, Eq. 7 can be solved by a least squares method, it often gets unstable because of the nature of the coefficient matrix $\mathbf{A}$. To deal with that, we have explained how to construct the optimal setup by selecting the color filter to be used in Section 3.3. Moreover, we employ a convex optimization technique to make the computation more stable.

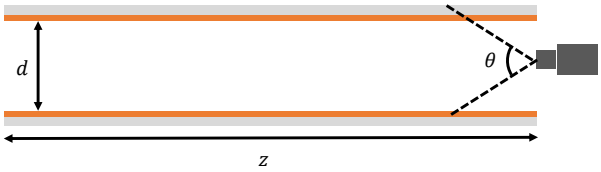

Figure 2: The setup of a coupled mirror.

The spectral reflectance physically can neither be a negative value nor over 1.0. This fact can be used as a strong box constraint. We can adopt a smoothness constraint on the spectral reflectance since it is often measured in the real world. Thus, we can rewrite Eq. 7 as

$$\hat{\boldsymbol{s}} = \arg\min_{\boldsymbol{s}} \left\{ \|\mathbf{A}\boldsymbol{s} - \boldsymbol{y}\|^2 + \alpha \int_\Lambda \left(\frac{\partial^2 s(\lambda)}{\partial \lambda^2} \right)^2 d\lambda \right\}, \quad \text{s.t.} \quad 0 \le s(\lambda) \le 1 \quad (\lambda \in \Lambda), \tag{9}$$

where α is the coefficient for the smoothness term. Then, Eq. 9 can be expressed in a matrix format as

$$\hat{\boldsymbol{s}} = \arg\min_{\boldsymbol{s}} \left\{ \|\mathbf{A}\boldsymbol{s} - \boldsymbol{y}\|^2 + \alpha \|\mathbf{D}\boldsymbol{s}\|^2 \right\}, \quad \text{s.t.} \quad 0 \le s_\lambda \le 1 \quad (\lambda_b \le \lambda \le \lambda_e), \tag{10}$$

where $\mathbf{D}$ is the second-order difference matrix. The objective function in Eq. 10 can be expressed in a quadratic program format as

$$\|\mathbf{A}\boldsymbol{s} - \boldsymbol{y}\|^2 + \alpha \|\mathbf{D}\boldsymbol{s}\|^2 = \boldsymbol{s}^{\mathrm{T}}(\mathbf{A}^{\mathrm{T}}\mathbf{A} + \alpha \mathbf{D}^{\mathrm{T}}\mathbf{D})\boldsymbol{s} - 2\boldsymbol{y}^{\mathrm{T}}\mathbf{A}\boldsymbol{s} + \boldsymbol{y}^{\mathrm{T}}\boldsymbol{y}. \tag{11}$$

Since the third term $\boldsymbol{y}^{\mathrm{T}}\boldsymbol{y}$ is constant, then Eq. 10 is equivalent to

$$\hat{\boldsymbol{s}} = \arg\min_{\boldsymbol{s}} \left\{ \boldsymbol{s}^{\mathrm{T}}(\mathbf{A}^{\mathrm{T}}\mathbf{A} + \alpha \mathbf{D}^{\mathrm{T}}\mathbf{D})\boldsymbol{s} - 2\boldsymbol{y}^{\mathrm{T}}\mathbf{A}\boldsymbol{s} \right\}, \quad \text{s.t.} \quad 0 \le s_\lambda \le 1 \quad (\lambda_b \le \lambda \le \lambda_e). \tag{12}$$

We solve Eq. 12 by using the quadratic cone programming technique [6]. To implement that optimization program, we utilize the python optimization library `cvxopt` [1].

4. Various setups as implementation

In Section 3, we have explained our technique of one-shot hyperspectral imaging by using faced mirrors. In order to implement the technique, various setups are available. In this section, we introduce two types of feasible setups by using a coupled mirror and a kaleidoscope.

4.1. Coupled mirror geometry

The simplest setup uses a pair of planar reflectors, faced to each other, on which color filters are attached. This setup is generally called a coupled mirror. First, we assume that the same filters are attached on both reflectors. Figure 2 illustrates the setup of a coupled mirror whose length is z and intervening distance is d. The angle of view of the camera is defined as θ. In this setup, the number of bounces N is geometrically limited to

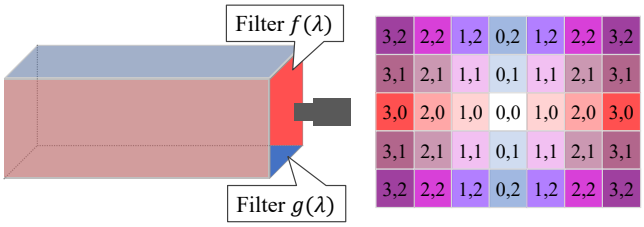

Figure 3: The setup of a kaleidoscope. Left: a quadrangular pole setup when two different color filters, whose spectra are $f(\lambda)$ and $g(\lambda)$, are used. Right: the combinations of (i, j) in Eq. 15 at a taken image.

$$N \le \left\lfloor \frac{z}{d} \tan \frac{\theta}{2} \right\rfloor. \tag{13}$$

Note that, in the actual setup, the number of bounces is also limited by the energy of the irradiance even if the right-hand side in Eq. 13 is a large number.

For instance, when an RGB camera whose angle of view is 120° and a coupled mirror whose length is 300mm and intervening distance is 10mm are used, $N \le 51$. The resolution of wavelength N_λ has to be less than or equal to $3N$ because the number of channels is three and the coefficient matrix $\mathbf{A}$ has to be a vertically long or square matrix for well-posedness. Therefore, the granularity of wavelength is limited to $d\lambda \ge \frac{\lambda_e - \lambda_b}{3N}$; that is, for example, it is theoretically possible to perform hyperspectral imaging at each 1.96nm wavelength, if the range is the visible light.

Secondly, we assume that two different color filters whose spectra are $f(\lambda)$ and $g(\lambda)$ are attached on the reflectors, respectively. In this case, Eq. 3 can be rewritten as

$$y_{k,i,j} = \int_\Lambda l(\lambda) s(\lambda) f^i(\lambda) g^j(\lambda) c_k(\lambda) d\lambda, \tag{14}$$

where $0 \le (i+j) \le N$. Since, geometrically, the reflection alternately happens on each reflector, $|i-j| \le 1$. Therefore, if $1 \le i \le \frac{N}{2} - 1$ then the patterns of j for each i are three; $j \in \{i-1, i, i+1\}$, and if $i \in \{0, \frac{N}{2}\}$ then the patterns are two. Totally, the number of combinations of (i, j) is $(\frac{3}{2}N - 2)$. In the case of using the same filter, the number of bounces represents the number of row vectors in the coefficient matrix. On the other hand, if the number of bounces is more than four, using two different filters makes the number of row vectors larger, and thus, the computation becomes more stable.

4.2. Kaleidoscope geometry

In computer vision, the kaleidoscope geometry has often been used to obtain many information by one-shot imaging for measuring the bi-directional texture function [13]

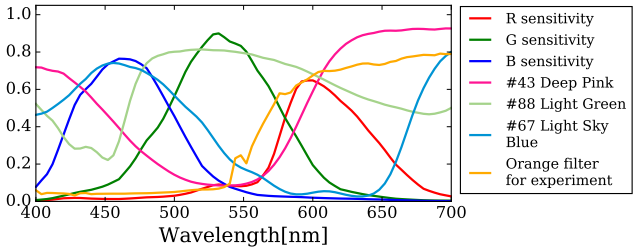

Figure 4: The spectral dataset.

and the shape [19] of an object. This approach can as well be useful for our technique of one-shot hyperspectral imaging. There are many kinds of kaleidoscope such as triangular pole, quadrangular pole, and hexagonal pole. Since our basic technique is based on a pair of reflectors, a setup consisting of multiple pairs of reflectors is a good match. Here, we introduce the quadrangular pole geometry as an implementation.

The quadrangular pole, shown in Fig. 3, consists of two pairs of reflectors. In principle, it is possible to use four different color filters but we only use two different filters whose spectra are $f(\lambda)$ and $g(\lambda)$. One kind of filter is attached on one of the pairs and another is attached on another of the pairs. Then, an observed intensity can be expressed as

$$y_{k,i,j} = \int_{\Lambda} l(\lambda)s(\lambda)f^{i}(\lambda)g^{j}(\lambda)c_{k}(\lambda)d\lambda, \qquad (15)$$

where $0 \leq i \leq N$ and $0 \leq j \leq N$. The number of combinations of (i, j) is naturally N^2, if the camera has the same horizontal and vertical angles of view. Generally, the vertical angle is less than the horizontal one, so the number of combinations can be lower but still is larger than that of a coupled mirror geometry configuration.

5. Experiments

5.1. Spectral dataset

We first explain the spectral dataset to be used in our experiments. In our experiments, we define the range of wavelength as the visible light, from 400 to 700nm. To generate synthetic data of spectral reflectance, we use a set of 1995 spectral reflectance including 350 surfaces Krinov dataset [18], 120 Dupont paint chips, 170 natural objects [30], 24 Macbeth color checker patches, 1269 Munsell chips, and 62 surfaces dataset [5]. We then measured the spectra of 253 Roscolux color filters and a thin clear orange filter for real data by using a spectrometer, OceanOptics Maya2000Pro. The spectral sensitivity of the camera, Nikon D5100, was estimated by the PCA-based method with data from [16, 17], as explained in [24]. Figure 4 shows the spectral sensitivity of the camera and the spectra of several of the color filters.

5.2. Synthetic data

We first perform experiments on synthetic data to validate our technique. Assuming a coupled mirror case with only one type of color filter, we simulated all observations for each bounce on each channel of the camera when using each of the 253 Roscolux filters and the thin clear orange filter. We repeated this simulation for observing each of the 1995 materials by Eq. 3. Then, we added zero-mean random Gaussian noise with a standard deviation of 0.1% onto the simulated intensities.

We reconstruct each spectral reflectance of the materials when using each of the filters by using Eq. 12. Then, we calculate their root-mean-square errors (RMSEs) to the ground truth for quantitative evaluation. The reconstructed results for the spectral reflectance of the Macbeth color checker are shown in Figs. 5 and 6 as examples, in which we used the thin clear orange filter and the #67 Light Sky Blue filter. As can be seen, the reconstruction results are mostly similar to the ground truth but the error at shorter wavelength is relatively larger. The condition numbers when using the thin clear orange filter and the #67 Light Sky Blue filter are 1.29×10^5 and 0.26×10^5, respectively. The #67 Light Sky Blue filter has the smallest condition number of the Roscolux color filters. The averages of RMSEs for the Macbeth color checker by using the thin clear orange filter and the #67 Light Sky Blue filter were 0.03 and 0.01, respectively. Since the maximum value of reflectance can be 1.00, the average reconstruction errors is 2% when using the thin clear orange filter. We will discuss this relationship between the condition number and the reconstruction error later. Then, we analyze the reconstruction errors from both perspectives of color filters and materials.

Figure 7 shows the average RMSE for reconstructing all materials when using each of the filters. After sorting in ascending order, we pick up 6 filters and then plot their spectra. This analysis explains what kind of filter is better in terms of smaller reconstruction error. As a result, a filter which allows a wide range of wavelengths and has higher gradients along wavelength is better as compared to a filter whose spectrum is very low or flat and has only one hump. Figure 8 shows the average RMSE for all filters when reconstructing each of the materials. We select 8 materials and then plot their spectral reflectance. This analysis shows what kind of material is difficult to be reconstructed. Results show that when the spectrum is smoother, the RMSE is smaller, but when if has a gap along wavelength, like the red line in Fig. 8, it is hard to be reconstructed. This is because of the smoothness constraint in Eq. 9.

Secondly, we analyze the relationship between condition numbers and reconstruction errors to verify our assertion mentioned in Section 3.3. We compute the condition number of coefficient matrix $\mathbf{A}$ when using each of the filters, and then compare that with the average RMSE for the fil-

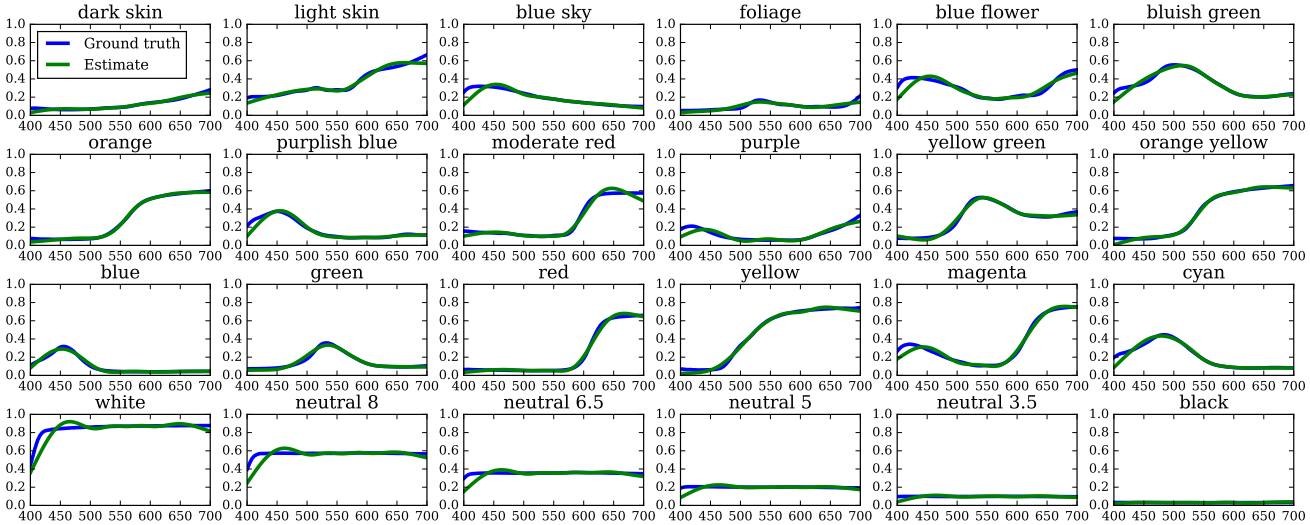

Figure 5: Experimental results on synthetic data for reconstructing the spectral reflectance of the Macbeth color chart in the spectral dataset when using the thin clear orange filter to be used in experiments on real data. The horizontal and vertical axes indicate wavelengths[nm] and reflectance, respectively.

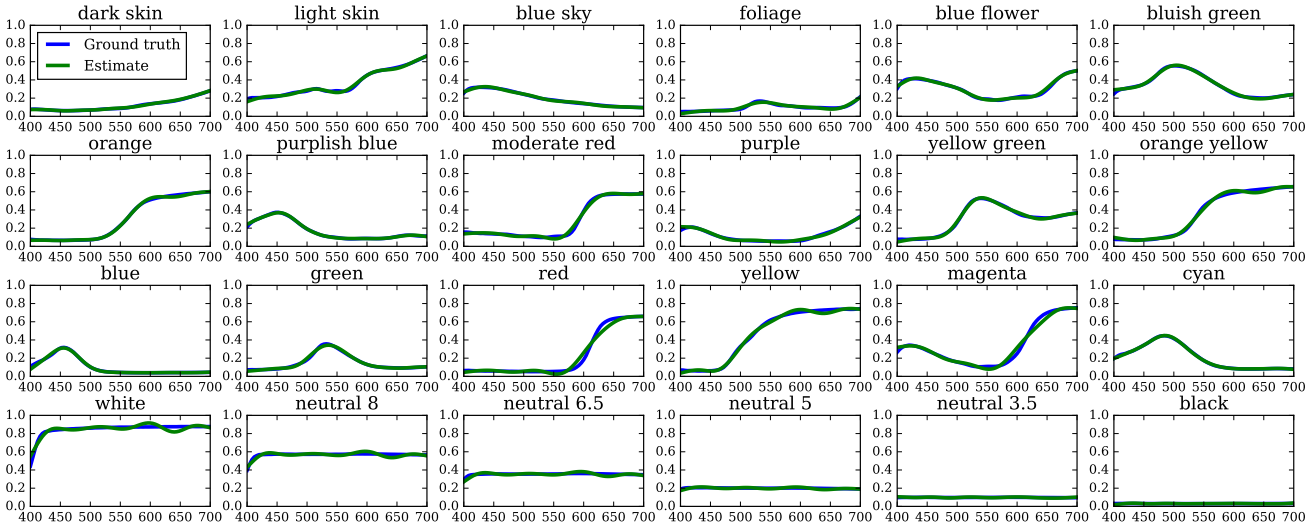

Figure 6: Experimental results on synthetic data for reconstructing the spectral reflectance of the Macbeth color chart in the spectral dataset when using the #67 Light Sky Blue filter in the Roscolux color filters. The horizontal and vertical axes indicate wavelengths[nm] and reflectance, respectively.

ter. Figure 9 shows the relationship between the condition numbers and the average RMSEs for all of the filters. It can be seen that the condition number is correlated with the average RMSE which supports our claim. This correlative relationship is helpful in selecting an optimal color filter.

5.3. Real data

After testing the proposed technique on synthetic data, we perform experiments on real data. We first implemented a simple setup which consists of two planar front surface reflectors and the thin clear orange filter, as shown in Fig. 10(a). All real data are taken by the camera Nikon D5100 under a white light source D65. Since the length of the reflectors is 100mm, the intervening distance is 20mm, and the angle of view is 120°, up to 8-th bounce reflections can be observed according to Eq. 13. Experimentally, it is only possible to observe up to 4-th bounce, as shown in Fig. 10(b), because of a physical interference between the camera and the setup.

To evaluate the accuracy of reconstructing spectral reflectance, we again use several chips on the Macbeth color chart, whose reflectance is known. As mentioned above, because only up to 4-th bounce can be observed, the number of total observations is 15, from 3 channels and 0 to 4-th bounces. This means that the granularity of wavelength is limited to 20nm. We reconstruct spectral reflectance in

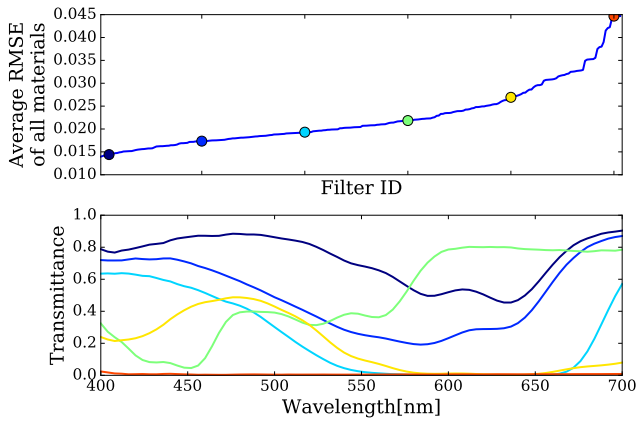

Figure 7: Analysis of the reconstruction errors for each filter. Top: the average RMSE for reconstructing all materials when using each of the 253 filters, sorted in ascending order. Bottom: the spectra of 6 filters chosen as color points on the top.

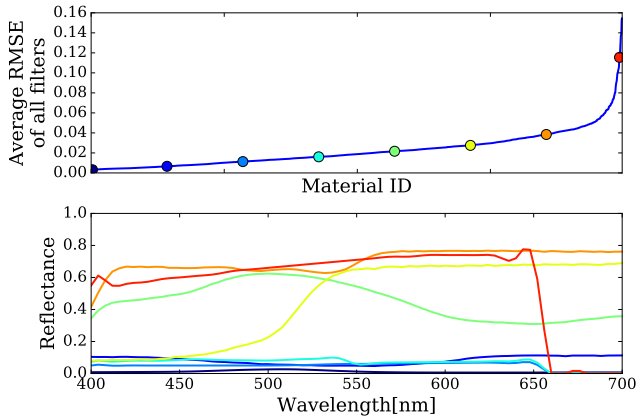

Figure 8: Analysis of the reconstruction errors for each material. Top: the average RMSE for all filters when reconstructing each of the 1995 materials, sorted in ascending order. Bottom: the spectral reflectance of 8 materials chosen as color points on the top.

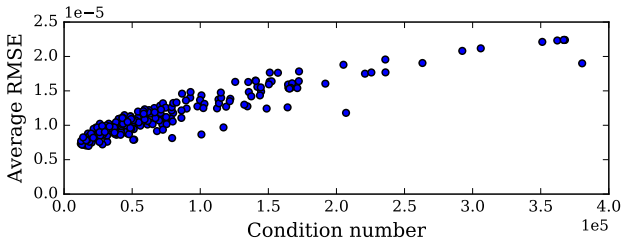

Figure 9: The relationship between the condition number of the coefficient matrix **A** and the reconstruction error. This shows the condition number is correlated to the reconstruction error.

30nm for stable computation. On each of yellow, red, and green chips, the pixel values are averaged to be used. Then, we reconstruct the spectral reflectance of those color chips. Figure 12 shows the spectral reflectance reconstructed by our technique and the ground truths. As a result, it can be

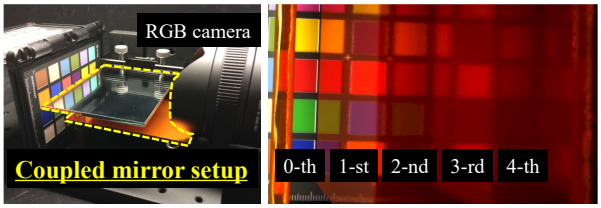

(a) (b)

Figure 10: Real setup. (a) coupled mirror setup consisting of two surface reflectors and the thin clear orange filter on the both reflectors. (b) a captured image by the camera where up to 4-th bounce can be seen.

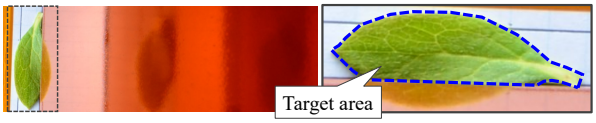

Figure 11: Experimental target: a green leaf. Left: a captured image by the camera with the real setup, where up to 2-nd bounce can be seen. Right: the area inside blue dash line is a target for reconstructing a hyperspectral image.

seen that the reconstruction results roughly fit to the ground truths for all color chips. The RMSEs for green, red, and yellow chips are 0.09, 0.13, and 0.20, respectively.

We finally perform a practical experiment for reconstructing a hyperspectral image. A target object is a green leaf, as shown in Fig. 11. When using the simple real setup, only up to 2-nd bounce can be observed because of the size of the leaf, so the number of total observations is nine. Furthermore, we can observe only a region inside blue bash line in Fig. 11 because of physical interference. Since it is necessary to perform geometric registration along all observed images, we put four markers in the scene and then compute homography transformation of the images. Figure 13 shows the hyperspectral image reconstructed by our technique and the ground truth captured by the hyperspectral camera SurfaceOptics SOC710. Note that the wavelengths indicated in Fig. 13 are not exactly same because the resolutions of wavelength are different between our method and the hyperspectral camera. Although only nine observations are available, our result has similar distributions to that of the ground truth, especially at 550 and 587nm. On the other hand, at shorter and longer wavelengths, the reconstructed images almost have no signal. This is because of the lack of observations and low signal-to-noise ratio.

6. Discussion

Our experimental results on synthetic data have shown that it is possible to reconstruct the accurate spectral reflectance by using a coupled mirror setup if the number of observations is large enough. A comparison between Figs. 5 and 6 shows that it is important to select the optimal color filter when the camera and the light source have been de-

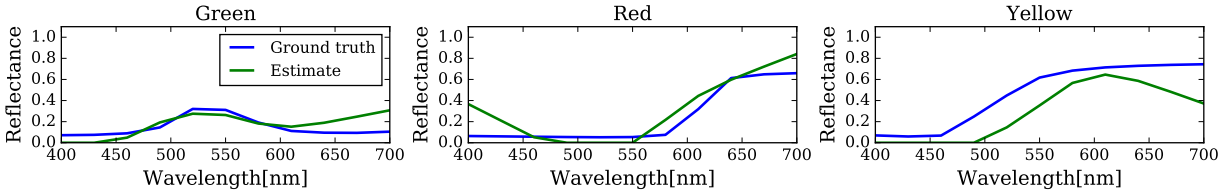

Figure 12: Experimental results on real data for reconstructing the spectral reflectance of green, red, and yellow chips on the Macbeth color chart.

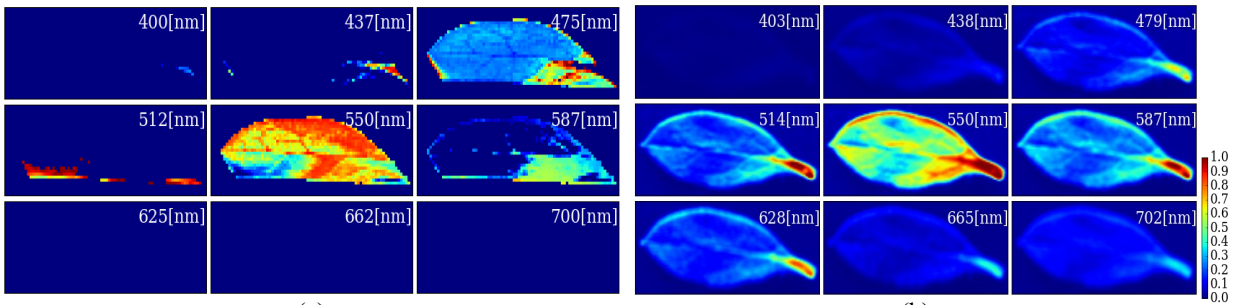

Figure 13: Experimental result on real data for reconstructing a hyperspectral image when capturing a green leaf. (a) the hyperspectral image reconstructed by our technique. (b) the ground truth hyperspectral image captured by SurfaceOptics SOC710. Reflectance is shown as pseudo-color. Note that the indicated wavelengths are different from each other because the resolutions of wavelength are different.

cided. In fact, it is difficult to observe many bounces in a real setup, as shown in the experiments on real data in Section 5.3. This is mainly because of two reasons: a) attenuation in light intensity and b) physical interference between the camera and the setup. Another problem comes from the color filter which is attached on the reflectors. Although we used a very thin filter, 2.5μm, the light was diffusely reflected a little and so the image after few bounces became unclear. This issue can be resolved by using thin color glass with a metallic sheet. While it is still difficult to obtain an accurate hyperspectral image as much as one by a commercial hyperspectral camera, the proposed technique can be used for capturing a very detailed spectral image around a certain wavelength, not whole wavelengths.

6.1. Trade-off and limitations

There is a trade-off between spectral and spatial resolutions. The trade-off is derived from the granularity of wavelength, $d\lambda \geq \frac{\lambda_e - \lambda_b}{3N}$. To obtain high spectral resolution, the number of bounces N needs to be enough large. However, it leads to a fact that the size of each bounce region in a image, which is equal to the spatial resolution, reduces. A way to make N larger is to shorten the intervening distance but it leads to a narrow field of view since the distance is equal to the field of view of the proposed setup.

Currently, the proposed setup has two limitations; low SNR after a number of bounces on the reflectors and only flat-surface objects as the target. Because of the low SNR, the variations of observations caused by a small number of observable bounces are limited but it can be resolved by using the kaleidoscope geometry with different color filters. Another way is to capture an image by a high dynamic range technique. Targeting a object with complex geometry is a challenging work because shape reconstruction is required to find corresponding between different bounce images. Those will be our future work.

7. Conclusion

In this paper, we have proposed a novel technique of one-shot hyperspectral imaging using faced reflectors, such as a coupled mirror and a kaleidoscope, on which color filters are attached. The key idea is based on that each of multiple reflections on the filters has a different spectrum, which allows us to observe multiple intensities through different spectra. We formulated an appearance model for faced reflectors. Then, we analyzed the nature of the coefficient matrix, which is one of our contribution in this paper, and showed that the condition number was correlated with the reconstruction error. Also, we analyzed the reconstruction errors to reveal what kind of filter should be used for a real implementation. In our experiments on real data, we showed the error of reconstructing spectral reflectance was on average 14% and performed hyperspectral imaging. The accuracy is still low but it supports our claim that one-shot hyperspectral imaging is feasible using faced reflectors with appropriate color filters.

Acknowledgments

This work was supported by JSPS KAKENHI Grant Number JP 17H04686.

References

[1] Cvxopt: Python software for convex optimization. http://cvxopt.org/. Accessed: 2016-11-12. 4

[2] F. M. Abed, S. H. Amirshahi, and M. R. M. Abed. Reconstruction of reflectance data using an interpolation technique. *Journal of the Optical Society of America A*, 26(3):613–624, 2009. 2

[3] A. Abrardo, L. Alparone, I. Cappellini, and A. Prosperi. Color constancy from multispectral images. In *Proc. of International Conference on Image Processing (ICIP)*, volume 3, pages 570–574. IEEE, 1999. 1

[4] G. R. Arce, D. J. Brady, L. Carin, H. Arguello, and D. S. Kittle. Compressive coded aperture spectral imaging: An introduction. *IEEE Signal Processing Magazine*, 31(1):105–115, 2014. 2

[5] K. Barnard, L. Martin, B. Funt, and A. Coath. A data set for colour research. *Color Research and Application*, 27(3):147–151, 2002. 5

[6] S. Boyd and L. Vandenberghe, editors. *Convex Optimization*. Cambridge University Press, 2004. 4

[7] C. Chi, H. Yoo, and M. Ben-Ezra. Multi-spectral imaging by optimized wide band illumination. *International Journal of Computer Vision*, 86(2-3):140–151, 2010. 2

[8] H. Du, X. Tong, X. Cao, and S. Lin. A prism-based system for multispectral video acquisition. In *Proc. of International Conference on Computer Vision (ICCV)*, pages 175–182. IEEE, 2009. 2

[9] M. D'Zmura. Color constancy: surface color from changing illumination. *Journal of the Optical Society of America A*, 9(3):490–493, 1992. 2

[10] K. Forbes, F. Nicolls, G. De Jager, and A. Voigt. Shape-from-silhouette with two mirrors and an uncalibrated camera. In *Proc. of European Conference on Computer Vision (ECCV)*, pages 165–178. Springer, 2006. 2

[11] N. Gat. Imaging spectroscopy using tunable filters: a review. In *Proc. SPIE Wavelet Applications VII*, pages 50–64, 2000. 2

[12] R. Habel, M. Kudenov, and M. Wimmer. Practical spectral photography. In *Computer graphics forum*, volume 31, pages 449–458. Wiley Online Library, 2012. 2

[13] J. Y. Han and K. Perlin. Measuring bidirectional texture reflectance with a kaleidoscope. *ACM Trans. on Graph.*, 22(3):741–748, 2003. 2, 4

[14] S. Han, I. Sato, T. Okabe, and Y. Sato. Fast spectral reflectance recovery using dlp projector. *International Journal of Computer Vision*, 110(2):172–184, 2014. 2

[15] M. Hinnrichs and M. A. Massie. New approach to imaging spectroscopy using diffractive optics, 1997. 2

[16] J. Jiang, D. Liu, J. Gu, and S. Süsstrunk. What is the space of spectral sensitivity functions for digital color cameras? In *IEEE Workshop on Applications of Computer Vision (WACV)*, pages 168–179. IEEE, 2013. 5

[17] R. Kawakami, Y. Matsushita, J. Wright, M. Ben-Ezra, Y.-W. Tai, and K. Ikeuchi. High-resolution hyperspectral imaging via matrix factorization. In *Proc. of IEEE Conference on Computer Vision and Pattern Recognition (CVPR)*, pages 2329–2336. IEEE, 2011. 5

[18] E. L. Krinov. Spectral reflectance properties of natural formations. Technical report, National Research Council of Canada, 1947. 5

[19] D. Lanman, D. Crispell, and G. Taubin. Surround structured lighting for full object scanning. In *Proc. International Conference on 3-D Digital Imaging and Modeling*, pages 107–116. IEEE, 2007. 5

[20] A. Manakov, J. Restrepo, O. Klehm, R. Hegedus, E. Eisemann, H.-P. Seidel, and I. Ihrke. A reconfigurable camera add-on for high dynamic range, multispectral, polarization, and light-field imaging. *ACM Trans. on Graph.*, 32(4):47–1, 2013. 2

[21] P. J. Miller and C. C. Hoyt. Multispectral imaging with a liquid crystal tunable filter. In *Photonics for Industrial Applications*, pages 354–365. International Society for Optics and Photonics, 1995. 2

[22] P. Morovic and G. D. Finlayson. Metamer-set-based approach to estimating surface reflectance from camera rgb. *Journal of the Optical Society of America A*, 23(8):1814–1822, 2006. 2

[23] R. M. Nguyen, D. K. Prasad, and M. S. Brown. Training-based spectral reconstruction from a single rgb image. In *Proc. of European Conference on Computer Vision (ECCV)*, pages 186–201. Springer, 2014. 2

[24] S. W. Oh, M. S. Brown, M. Pollefeys, and S. J. Kim. Do it yourself hyperspectral imaging with everyday digital cameras. In *Proc. of IEEE Conference on Computer Vision and Pattern Recognition (CVPR)*, pages 2461–2469, 2016. 2, 5

[25] J.-I. Park, M.-H. Lee, M. D. Grossberg, and S. K. Nayar. Multispectral imaging using multiplexed illumination. In *Proc. of International Conference on Computer Vision (ICCV)*, pages 1–8. IEEE, 2007. 2

[26] I. Reshetouski, A. Manakov, H.-P. Seidel, and I. Ihrke. Three-dimensional kaleidoscopic imaging. In *Proc. of IEEE Conference on Computer Vision and Pattern Recognition (CVPR)*, pages 353–360. IEEE, 2011. 2

[27] D. W. Stein, S. G. Beaven, L. E. Hoff, E. M. Winter, A. P. Schaum, and A. D. Stocker. Anomaly detection from hyperspectral imagery. *IEEE Signal Processing Magazine*, 19(1):58–69, 2002. 1

[28] S. Tominaga. Multichannel vision system for estimating surface and illumination functions. *Journal of the Optical Society of America A*, 13(11):2163–2173, 1996. 2

[29] S. Tominaga and R. Okajima. Object recognition by multispectral imaging with a liquid crystal filter. In *Proc. of International Conference on Pattern Recognition (ICPR)*, volume 1, pages 708–711. IEEE, 2000. 1

[30] M. J. Vrhel, R. Gershon, and L. S. Iwan. Measurement and analysis of object reflectance spectra. *Color Research and Application*, 19(1):4–9, 1994. 5